Nanoscale

Accepted Manuscript

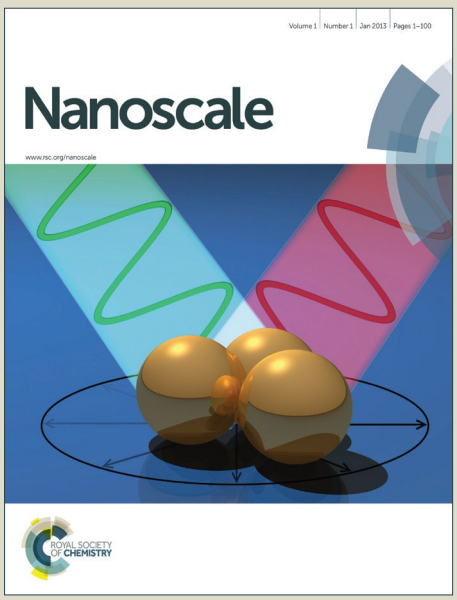

ROYAL SOCIETY OF CHEMISTRY

www.rsc.org/nanoscale

Cite this: DOI: 10.1039/c0xx00000x

www.rsc.org/xxxxxx

PAPER

pH-sensitive self-assembling nanoparticles for tumor near-infrared fluorescence imaging and chemo-photodynamic combination therapy

Wenxiu Hou[a,b], Xin Zhao[a] ,Qiao qing Qian[a,b], Fei Pan[a], Chunlei Zhang[a], Yuming Yang[a], Jesús Martínez de la Fuente[a,c], Daxiang Cui [a]*

Received (in XXX, XXX) Xth XXXXXXXXX 20XX, Accepted Xth XXXXXXXXX 20XX
DOI: 10.1039/b000000x

Development of visual tumor theranostic nanoparticles has become a great challenge. In this study, D-α-tocopheryl polyethylene glycol 1000 succinate (TPGS) was conjugated to acid-sensitive *cis*-aconitic anhydride-modified doxorubicin (CAD) to obtain a pH-sensitive anti-tumor prodrug nanoparticles (TCAD NPs) via self-assembling. Subsequently, the photosensitizer chlorin e6 (Ce6), was loaded into the resulting prodrug nanoparticles to prepare a novel tumor near-infrared fluorescence imaging and chemo-photodynamic combination therapy system (TCAD@Ce6 NPs). An accelerated release of doxorubicin (DOX) and chlorin e6 (Ce6) from the TCAD @Ce6 NPs could be achieved due to the hydrolysis of the acid-sensitive amide linker under mild acidic conditions (pH=5.5). *In vitro* experiment showed that A549 lung cancer cells exhibited a significantly higher uptake of DOX and Ce6 by using our delivery system than the free form of DOX and Ce6. *In vivo* experiment showed that TCAD@Ce6 NPs displayed better tumor targeting gathering through the enhanced permeability and retention (EPR) effect than free Ce6, thus improving fluorescence imaging. Moreover, chemo-photodynamic combination therapy of TCAD@Ce6 NPs combined with near-infrared laser irradiation was confirmed to be capable of inducing high apoptosis and necrosis of tumor cells (A549) *in vitro* and to display a significantly higher tumor growth suppression in A549 lung cancer-bearing mice model. Furthermore, compared with exclusive chemo treatment (DOX) or photodynamic treatment (Ce6), our system showed enhanced therapeutic effects both *in vitro* and *in vivo*. In conclusion, the high performance TCAD@Ce6 NPs can be used as a promising NIR fluorescence imaging and high effective chemo-photodynamic system for theranostics of lung cancer, etc. in near future.

Introduction

Lung cancer has become No.1 leading cause of death worldwide and the number of lung cancer patients is rising remarkably.[1] Current cancer therapeutic methods mainly include surgery, chemotherapy, radiotherapy and immunotherapy. Doxorubicin (DOX) is a highly effective chemotherapeutic drug used to treat a wide variety of tumors such as breast cancer, prostate cancer, brain cancer and lung cancer, etc.[2, 3] Furthermore, DOX with anthracycline can interact with DNA to block gene replication and transcription.[4, 5] However, free DOX was not widely used in chemotherapy due to its short half-life and cytotoxicity to important organs such as heart, kidney, etc.[6, 7] Therefore, it is very necessary to develop novel efficient delivery formulations of DOX to improve its clinical efficacy and safety. Up to date, numerous DOX delivery systems have been developed to improve antitumor therapeutic efficacy of DOX, including nanoparticles,[8] intelligent micelles,[4] liposomes,[9] and dendrimers.[10] Nonetheless, the chemotherapy is accompanied by several side effects derived from its toxicity and terrible pain, making this treatment far from ideal. Scientists have already taken advantage of combined therapy to boost therapeutic efficiency and simultaneously reduce the side effects of cancer chemotherapy.[11-14]

In recent years, photodynamic therapy (PDT), another effective cancer treatment method, has attracted broad attention. The principle of PDT treatment is that certain photosensitive compounds can produce highly reactive oxygen species (ROS) upon photoexcitation which irreversibly induce cell apoptosis or necrosis in the targeted tissue.[15] In addition, because these photosensitizers also emit fluorescence signal under light excitation, they can serve as a contrast agent for tumor fluorescence imaging.[16] Although PDT has been used to treat some tumors, the potential of photosensitizers to become widely applied to cancer therapy is still hampered by many limitations such as water-insolubility and low tumor targeted accumulation.[17, 18] To overcome these drawbacks of photosensitizers of PDT, various nanoparticle-based systems have been developed to enhance the tumor targeting and PDT efficacy of photosensitizers.[9, 19, 20] Moreover, based on the attractive tumor therapy properties of PDT, the combined treatment of photodynamic and chemotherapy may optimize cancer treatment and achieve enhanced antitumor efficiency. Chlorin e6 (Ce6) is one of those promising photosensitizers, and

it has been approved as a tool for photodynamic diagnostics in clinical application by FDA.[21, 22] As its high singlet oxygen quantum yield and absorption/emission wavelength in NIR region it can induce necrosis of tumor by deeper tissue penetration, therefore, Ce6 should be excellent photosensitizer for PDT.[23-26] In addition, TPGS is a water-soluble amphiphilic macromolecule derived from natural vitamin E, and it has been widely used as an effective emulsifier or solubilizer.[27-29] TPGS is characterized by its bulky nature, water-soluble, and large surface area, that makes it a good candidate to serve as a promising drug delivery system to enhance the solubility and bioavailability of anticancer drug. Actually, since FDA approved its clinic application, as a safe drug delivery system, it was widely used in cancer therapy with a high chemotherapy efficacy and low toxic side effects.[30-32] Therefore, in order to optimize chemotherapy efficacy of doxorubicin (DOX) and improve fluorescence diagnosis and PDT efficacy of photosensitizer chlorin e6 (Ce6), we firstly focus on developing D-α-tocopheryl polyethylene glycol 1000 succinate (TPGS) as the carrier of the hydrophobic chemotherapeutic agent doxorubicin (DOX) and photosensitizer chlorin e6 (Ce6) for simultaneous tumor near-infrared fluorescent imaging and chemo-photodynamic combination therapy. Briefly, pH-sensitive cis-aconitic anhydride (CA)-modified DOX was firstly synthesized (CAD), then, the hydroxyl terminal group of TPGS was bond with the carboxyl group of cis-aconitic anhydride (CA)-modified DOX to synthesize the pH-responsive prodrug nanoparticles (TCAD NPs) via self-assembling in aqueous solution (Figure S1 & Scheme 1). Subsequently, chlorin e6 (Ce6) was loaded into the resulting prodrug nanoparticles to prepare the TCAD@Ce6 nanoparticles (TCAD@Ce6 NPs), with TPGS as hydrophilic shell, and chlorin e6 and Dox as hydrophobic core. As the existential pH value of tumor tissue, intracellular endosomal and lysosomal is lower than physiological condition,[5, 33] TCAD@Ce6 NPs via the acid-sensitive amide linker to achieve the "OFF/ON" switch. Under ideal circumstances, our theranostic nanoparticles would not leak Dox and would self-quenched the fluorescence of Ce6 by π–π interactions in the blood circulation. Due to the enhanced permeability and retention (EPR) effect, TCAD@Ce6 NPs could be gradually accumulated into the tumor location, where TCAD@Ce6 NPs could be activated to rapidly release DOX and Ce6 (Scheme1) improving tumor NIR imaging, and enhancing chemo-photodynamic therapy.[19] In these studies the physicochemical properties, cellular uptake efficacy, *in vitro* phototoxicity, *in vivo* tumor targeting efficacy, and *in vivo* therapeutic efficacy of TCAD@Ce6 NPs were evaluated. Results showed that the developed acid-sensitive TCAD@Ce6 NPs displayed enhanced anti-tumor activity, specific tumor targeting and enhanced fluorescence imaging efficacy. Therefore, the exploited acid-sensitive TCAD@Ce6 NPs exhibite great potential in applications such as tumor NIR fluorescence imaging and simultaneous chemo-photodynamic therapy in near future.

Experimental

Materials

Doxorubicin was obtained from Dalian Meilun Biotech Co., Ltd (Dalian, China). D-alpha tocopherol acid polyethylene glycol succinate (TPGS) was purchased from Ai Keda Chemical Technology Co., Ltd. (Chengdu, China). Dihydro-2, 5-dioxofuran-3-acetic acid (CA) was received from Meryer Chemical Technology Co., Ltd. (Shanghai, China). N, N′-dicyclohexylcarbodiimide (DCC), N hydroxysuccinimide (NHS), Triethylamine (TEA), anhydrous dimethyl sulfoxide (DMSO), and tetrahydrofuran (THF) were purchased from Aladdin Reagent Co., Ltd. (Shanghai, China). 3-[4, 5-dimethylthiazol-2yl]-2, 5-diphenyltetrazolium bromide (MTT) was obtained from Sigma Chemical Corporation (USA). Annexin V-FITC/PI Apoptosis Detection Kit was purchased from Yeasen Corporation (Shanghai, China). Hoechst 33342 and, 2′, 7′-dichlorofluorescein diacetate (DCFH-DA), were purchased from Invitrogen Corporation (Carlsbad, CA, USA). Chlorin e6 (Ce6) was obtained from Frontier Scientific (Utah, USA). All other chemicals were of reagent grade. Water was purified with Milli-Q Plus 185 water purification system (Millipore, Bedford, MA).

Preparation of the TCAD nanoparticles

Cis-aconitic anhydride modified doxorubicin (DOX) was prepared as previously reported with some changes.[34] Doxorubicin hydrochloride (DOX·HCl) with twice the molar concentration of triethylamine (TEA) were dissolved in DMSO. The mixture was stirred overnight light-protected at room temperature to obtain doxorubicin base (DOX). Cis-aconitic anhydride (50 mg) dissolved in 5 mL of dioxane was added dropwise to DOX (50 mg, previously dissolved in 5 mL of pyridine) under intensive stirring. The reaction mixture was stirred overnight at 4℃ protected from light. After that, the products were extracted five times with 10 mL chloroform and 10 mL 5% sodium bicarbonate (aqueous solution). Then, the precipitate present in the aqueous phase was removed by centrifugation at 4℃ (10000 rpm, 5 min). The pH of the supernatant was adjusted by adding hydrochloric acid (1 N) until the precipitate was separated out (pH about 2.5-3.0). Then, the solution was stirred for another extra 30 min to collect the precipitate by centrifugation at 4℃ (10000 rpm, 10 min). The precipitate was washed with distilled water to remove the saline solution. The final product, referred as ''N-cis-aconityl doxorubicin (CAD)'', was dried by lyophilisation . The yields of CAD were 50 %.

Synthesis of TPGS-CAD conjugates: CAD (20 mg) was dissolved in 5 mL DMSO stirred for 30 min and then EDC·HCl (27.79 mg), DMAP (2.12 mg), and DCC (11.95 mg) were added to the CAD solution and incubated for about additional 3 h to activate carboxyl of CAD. TPGS (39.8 mg) was dissolved in 2 mL DMSO, added dropwise to the solution and incubated for 24 h. Both steps were incubated in the dark at 38℃. The insoluble byproduct (dicyclohexylurea) was removed by filtration of the reaction mixture. The filtrate was separated by dialysis (MWCO 3500) against PBS (pH 8.0) for 1 day, and then against ultrapure water for 2 days. The final product, referred as "TPGS-CAD conjugate (TCAD)" was dried by lyophilization . The yields of TCAD were 67 %.

Preparation of TCAD nanoparticles: In brief, 5 mg TCAD was dissolved in 2 mL of tetrahydrofuran (THF), then 8 mL deionized water was dropwise into the above solution. The reaction solution was stirred at room temperature for 30 min. Whereafter, the THF was removed by rotary evaporation, the residue was resuspended

in deionized water, followed by filtering through a 0.45 μm pore-sized microporous membrane.

Preparation of TCAD@Ce6 nanoparticles.

Chlorin e6 (Ce6) was loaded into TCAD using a simple dialysis method. Briefly, Ce6 (2 mg) dissolved in 1 ml of 1:1 (v/v) THF/DMSO was slowly added to TCAD (15 mg) dissolved in 6 mL of distilled water. The mixed solution was thereafter sonicated for 30 min at 100 W. Then the solution was stirred at room temperature for 12 h light-protected. The product was separated by dialysis (MWCO 3500) against 0.1 M $NaHCO_3$ for 12 h, and then against ultrapure water for 2 days. The Ce6 loading capacity was estimated by the ultraviolet absorbance at 660nm (Figure S2(B), ESI) of Ce6.[35] The final product was filtered through a 0.45μm pore-sized microporous membrane.

The Entrapment Efficiency (EE) and Drug-Loading capacity (DL) were calculated using the following equations:

EE (%) = weight of Ce6 in nanoparticles /weight of Ce6 fed initially ×100%;

DL (%) = weight of Ce6 in nanoparticles/weight of Ce6 in nanoparticles and weight of carriers ×100%;

Characterizations

The size and morphology of the TCAD NPs and TCAD@Ce6NPs were characterized by TEM on a JEM-2100F (JEOL, Japan). The size and morphology of TCAD NPs were also measured by field emission scanning electron microscopy (FESEM: ZEISS). UV-Vis spectra were measured with a Varian Cary 50 spectrophotometer (Varian Inc., Palo Alto, CA, USA). PL spectra were recorded on a Hitachi FL-4600 spectro fluorometer. DLS (dynamic light scattering) measurements were completed using a NICOMP 380 ZLS Zeta potential/Particle sizer (PSS Nicomp, Santa Barbara, CA, USA). ^{1}H NMR spectra were acquired using a Bruker Avance-III-HD 600 MHz NMR Spectrometer (Bruker BioSpin Corp., Billerica, MA, USA). Fourier transform infrared (FT-IR) spectra were recorded on a Bio-Rad WinIR instrument using potassium bromide method.

Critical aggregation concentration (CAC) measurement

Pyrene was used for the fluorescence probe to determine the CAC value of the TCAD NPs. 1μL of pyrene acetone solution (6×10^{-4} mol/L) was added to 1 mL of TCAD aqueous solution with different concentrations. The mixture was sonicated for 30 min and then was incubated for extra 12 h in the dark at room temperature. The fluorescence intensity of the emission wavelengths (λ em) of 384 nm (I3) and 373 nm (I1) of all samples were recorded on a Hitachi FL-4600 spectro fluorometer at 336 nm excitation wavelength and 5 nm slit width. The I3/I1 values of all samples were calculated and analyzed as a function of logarithm of the nanoparticles concentration.

Measurement of *in vitro* DOX and Ce6 release

To evaluate the *in vitro* release profiles of DOX and Ce6 from TCAD@Ce6 NPs, 2 mL of TCAD @Ce6 NPs (0.5 mg/mL) was dissolved in PBS and subsequently transferred into a membrane tubing (MWCO 3500 Da). It was incubated in 80 mL PBS at pH 7.4 (a mimicking normal physiological condition), pH 6.5(a tumor tissue acidic microenvironment) and pH 5.5 (an intracellular acidic microenvironment), with continuous shaking of 100 rpm at 37 ℃, respectively. At predetermined time intervals, 1 mL of release medium was taken out, and an equal volume of fresh PBS was returned to the system. The accumulative amount of the released DOX and Ce6 was detected by UV-Vis spectra at 480 nm for DOX and at 660 nm for Ce6.

TCAD@Ce6 NPs (4 μg/mL of Ce6 equivalents) in DMEM medium with 10% FBS were incubated with or without A549 cells for different time at 37℃ to detect the fluorescence intensity changes of TCAD@Ce6 NPs in tumor cells. Near-infrared (NIR) fluorescence images were then recorded with Bruker In-Vivo F PRO imaging system. Moreover, the fluorescence intensity changes of TCAD@Ce6 NPs were also measured by PL spectra before and after its incubated at 37℃ in PBS (pH 5.5) for 24 h.

Cell culture

The human non-small cell lung cancer cells (A549 cells) were used for cell studies. A549 cells were incubated in DMEM medium with 10% FBS at 37 ℃ with 5% CO_2. Before experiments, the cells were pre-cultured until 75% confluence was reached.

***In vitro* cellular uptake and distribution of TCAD**

For confocal microscopy experiments: A549 cells were plated onto coverglass in 24-well plates at a density of 2.0×10^4 cells per well and allowed to adhere for 24 h. Then, the culture medium was replaced by a fresh one containing 4 μg/mL free Ce6, 5.86 μg/mL free dox, TCAD NPs (5.86 μg/mL of DOX equivalents), or the TCAD@Ce6 NPs (4 μg/mL of Ce6 equivalents, 5.86 μg/mL of DOX equivalents). After 4 h and 12 h co-incubation, the cells were washed twice with PBS sufficiently and then fixed with 2.5 % glutaraldehyde at 4 ℃ for 30 min. The nuclei of the cells were stained with Hoechst 33342 at room temperature for 15 min. Confocal fluorescence imaging studies were performed with a TCS SP8 confocal laser scanning microscopy. Hoechst 33342 was excited using the blue diode 405 nm laser and the emission was recorded between 440 and 470 nm. Ce6 was excited at 633 nm and the emission was collected from 650 to 800 nm. DOX was excited at 488 nm and the emission was collected from 500 to 590 nm.

Flow cytometry (BD FACSCalibur) measurements to quantify the cellular uptake: A549 cells (1.0×10^5 cells per well in 6-well plates) were cultured in medium for 24 h, and co-incubated with free Ce6, free dox, TCAD NPs or TCAD@Ce6 NPs (with the same concentrations of confocal fluorescence imaging studies) for 4 h and 12 h, respectively. Whereafter, the cells were washed with PBS and then the cells were trypsinized and resuspended in 0.5 mL of PBS for flow cytometry measurements. The flourescence signal of Ce6 and DOX were collected by FL3-H and FL1-H channel, respectively.

Cell viability and apoptosis assay

Cellular ROS (reactive oxygen species) detection during irradiation: The intracellular ROS generation was monitored by staining all the cells with DCFH-DA. The A549 cells were incubated with PBS, free Ce6 (4 μg/mL) or TCAD@Ce6 NPs (equivalent Ce6 4 μg/mL) in six-well plate. After 24 h co-culture, the cells were further incubated with 20 μM DCFH-DA for 20 min and irradiated using a 633 nm He-Ne laser at a power of 50 mW/cm^2 for 3 min or not. Subsequently, the fluorescence intensity of DCF inside the cells was detected by flow cytometry,

which on behalf of the amount of ROS produced.

In addition, the singlet oxygen sensor green (SOSG) reagent, which was highly selective for $^1O_2$, was employed to measure the $^1O_2$ generation of the TCAD@Ce6 NPs (equivalent Ce6 4μg/mL) in different irradiating times at 633 nm (50 mW/cm^2) (excitation= 494 nm).

MTT assay: The dark toxicity and phototoxicity of free Ce6 and TCAD@Ce6 NPs were determined by MTT assay of A549 cells. Briefly, A549 cells were seeded in 96-well plate at a density of 5×10^3 cells per well. After 24 h incubation, the cells were incubated with 100 μL fresh complete medium containing serial concentrations of free Ce6 (0.1-4 μg/mL) or TCAD@Ce6 NPs (equivalent Ce6 0.1-4 μg/mL) or PBS (control group). After incubation for 12 h at 37 ℃ in the dark. The cells were washed twice with fresh medium, one plate was kept in the dark to study dark toxicity, and the other plate was irradiated using a 633 nm helium-neon (He-Ne) laser at a power of 50 mW/cm^2 for 1.5 min and 3 min, respectively. After extra 12 h of incubation in dark, the dark toxicity and phototoxicity was evaluated by MTT assay. The cell viability was calculated according to the equation: Cell viability = (OD 570 nm of the experimental group/OD 570 nm of the control group) ×100% and the cell viability of control group were denoted as 100%. According to the above protocol, MTT assay was also carried out to evaluate the cytotoxicity of free DOX and TCAD NPs. The A549 cells were incubated with 100 μL fresh complete medium containing serial concentrations of free DOX (0.1-6 μg/mL) and TCAD NPs (equivalent DOX 0.1-6 μg/mL) for 24 h and 48 h, respectively, before execution the MTT assay.

Visually observe the photodynamic therapeutic efficacy: The A549 cells were seeded onto a 24-well plate (1×10^4 cells per well), then incubated for 24 h. The medium was replaced with fresh medium containing TCAD@Ce6 NPs (equivalent Ce6 4 μg/mL), or the free Ce6 (4 μg/mL). After 12 h incubation in the dark, the A549 cells were changed to fresh culture medium, irradiated with or without an NIR laser (633 nm, 50 mW cm^2) for 3 min. After another 12 h incubation in the dark, the cells were washed with PBS and stained with Calcein-AM and PI. The live cells and dead cells were stained by Calcein-AM and PI, respectively.

Apoptosis Assay: The apoptotic and necrotic cell distribution were tested according to the manufacturer's instruction of Annexin V-FITC/PI Apoptosis Detection Kit. The A549 cells exposed to free Ce6 (4 μg/mL) or the TCAD@Ce6 NPs (equivalent Ce6 4 μg/mL) for 12 h. Then, the cells were washed twice with 1×PBS and the medium was replaced with fresh complete culture medium, followed by irradiated with or without a 633 nm He-Ne laser at a power of 50 mW/cm^2 for 3 min. Afterward, the cells were trypsinized, harvested, washed with 1×PBS and resuspended in 190 μL of binding buffer. Finally, the cells were stained with 5 μL Annexin V and 5 μL PI in dark at room temperature for 15 min. 300 μL of binding buffer was added to each sample before the cells were analyzed by BD FACSCalibur within 30 min. The data was analyzed by FlowJo 7.6 software.

Tumor-targeting efficiency in tumor bearing mice

Female BALB/c-nude mice (4 weeks of age) were purchased from Shanghai Slac Laboratoty Animal Co., Ltd (Shanghai, China). All animals received care in compliance with the Institutional Animal Care and Use Committee of Shanghai Jiao Tong University. The female nude mice were injected subcutaneously in the right flank region with 150 μL of cell suspension containing 4×10^6 A549 cells. The tumors were allowed to grow to reach a size of ~200 mm^3 before the biodistribution and imaging studies. Free Ce6 or TCAD@Ce6 NPs in saline (at a dosage of Ce6 4mg/kg of total mouse body weight) were intravenously injected into the tumor-bearing mice. Fluorescent images were taken at 2, 4, 12, and 24 h after injection by a Bruker In-Vivo F PRO imaging system (Billerica, MA, USA) (excitation: 630/20 nm; emission: 700/30 nm; integration time: 10 s). The mice were sacrificed, tumors and major organs were collected at 24 h post injection. Excised tumors and organs were imaged by the Bruker In-Vivo F PRO imaging system with the same parameters as mentioned above. The average fluorescence intensity of tumors and other organs were quantified by Bruker Molecular Imaging Software 7.1 Version.

Photodynamic therapeutic efficacy of TCAD@Ce6NPs in tumor-bearing mice

In vivo chemotherapy, photodynamic and chemo-photodynamic treatments were performed using A549 tumor-bearing mice. When the tumor size reached ~100 mm^3, the mice were randomized into six groups of 3 animals per group. (1) PBS (150 μL) without laser, (2) PBS (150 μL) with laser, (3) free Ce6 (4 mg/kg) upon laser irradiation, (4) free dox (5.86 mg/kg), (5) TCAD NPs (equivalent dox 5.86 mg/kg) and (6) TCAD@Ce6 NPs (4 mg/kg of Ce6 equivalents, 5.86 mg/kg of DOX equivalents) with laser irradiation were injected into the tail vein ， respectively. For the irradiated groups, a 633 nm He-Ne laser (50 mW/cm^2, 30 min) was used after 12 h of intravenous injection. The day 0 showed the day of intravenous injection was administered, and the 1 day on behalf of the 12 h after irradiation. The tumor size and body weight were measured by a caliper and electronic balance every three days after treatment, respectively. The tumor volumes = a × (b) $^2\times1/2$, where a and b represent the maximum length and the minimal width of tumors, respectively. On day 18, the mice treated with TCAD@Ce6 NPs were sacrificed. Heart, liver, spleen, lung, and kidney were excised and further investigated after H&E staining to monitor the morphological features of each organ.

Results and discussion

Synthesis and characterization

To render the formed delivery system with acid-sensitive properties for tumor specific drug release, acid-sensitive cis-aconitic anhydride-modified DOX (CAD) was firstly prepared through the ring-opening reaction.[4] (Figure S1, Electronic Supplementary Information, ESI). As shown in ^{1}H NMR spectra (Figure 1A-DOX), the peak at about 7.9 ppm belongs to the protons of the anthracene moiety of DOX. After cis-aconitic anhydride modification, additional signals at 6.1 and 6.4 ppm appeared, attributed to the protons (CH-COO-) of the cis-aconitic anhydride linkages in the structure of Cis-DOX (Figure 1A-CAD). Surface TPGS modification is demonstrated to further improve the cellular uptake and increase the half-life as well as the therapeutic effects of the drug.[36] Therefore, in this study we

modified CAD with TPGS by ester linkage (Figure S1, ESI). ^{1}H NMR spectra of TPGS and TCAD displayed an intense signal at around 2.0 ppm, attributed to the protons of succinyl methylene (Figure 1B). Also, the characteristic peak of TPGS at 3.5 ppm belonging to methylene protons of the *m*PEG part can be observed in both spectra of TPGS and TCAD (Figure 1B). Because of the relative small molecular weight of CAD, we could only see the much weaker intensity of CAD characteristic proton signals at around 8.0, 13.2, and 14.0 ppm (Figure 1B insert) compared with that of TPGS. FT-IR spectra were further used to confirm the structure of these formed compounds as shown in Figure 1C. The signals that appeared at around 1548 cm^{-1} (Amide II) in CAD were assigned to the characteristic signals of the formed amide bond. After the TPGS modification, the new absorption bands at 1111 cm^{-1} was attributed to stretching modes of -CH2-O-CH2- of the TPGS, while the typical absorption bands at 3440 and 1633 cm^{-1} were associated with the stretch of the phenolic hydroxyl group and amide I of CAD. Moreover, the small peaks at 1695 and 1584 cm^{-1} indicated the formation of the ester group between TPGS and CAD (Figure 1D). The TCAD was also characterized by ultraviolet-visible spectrophotometry (UV-Vis) (Figure S2(A), ESI). All of the above experiments confirmed the successful synthesis of TCAD. In water, the amphiphilicity character of the TCAD allows it to self-assemble into nanoparticles, which insoluble DOX as the hydrophobic core and hydrophilic TPGS as shell. To acquire tumor targeting fluorescence imaging and chemo-photodynamic combination therapy, chlorin e6 (Ce6) was loaded into the TCAD NPs to form the TCAD@Ce6 NPs via self-assembly process. The loading efficacy, encapsulation efficiency and hydrodynamic diameter were altered with the change of D/P ratios (Table 1). To obtaine highly Ce6 loading ratio and reduce the waste of the Ce6, the D/P ratio of 20% was selected for further studies. The loading efficacy determined by UV-Vis spectroscopy was about 14.89 %. The absorbance spectra of TCAD NPs, free Ce6 and TCAD@Ce6 NPs were measured by UV-Vis spectroscopy. TCAD@Ce6 NPs have a characteristic absorption peak of DOX at 480 nm and a bathochromic absorption peak of Ce6 at 659 nm (Figure S2(B), ESI). The bathochromic shift of absorption peak of Ce6 may response to the changes of the Ce6 environment.[37] As a result, the Ce6 was successfully encapsuled into the TCAD NPs.

The hydrodynamic diameter of TCAD NPs (196.0 nm) and TCAD@Ce6 NPs (160.0 nm) in the range of 50-200 nm (Figure S3(A), ESI & Figure 2A, insert), indicated that TCAD NPs and TCAD@Ce6 NPs may preferentially distribute into the tumor by the enhanced permeability and retention (EPR) effect.[38, 39] The morphology of the dried TCAD NPs and TCAD@Ce6 NPs was evaluated by transmission electron microscopy (TEM). The TEM image results proved that the TCAD NPs and TCAD@Ce6 NPs were almost spherical and uniform with good monodispersity (Figure 2A & Figure S2(B), ESI). Moreover, the scanning electron microscope (SEM) imaging of TCAD NPs showed the similar result of TEM (Figure S3(C), ESI). The size of TCAD@Ce6 NPs was smaller than TCAD NPs that may owe to the addition of Ce6, that increases the hydrophobic interaction during the self-assembly process. More importantly, The results of hydrodynamic diameter measured at fixed time points during a month indicated that the sizes of TCAD NPs and TCAD@Ce6 NPs fluctuates in small scope, suggesting that both TCAD NPs and TCAD@Ce6 NPs are stable and can be stored in water for relativelly long periods of time without sedimentation or aggregation (Figure 2B). The critical aggregation concentrations (CACs) of TCAD NPs were determined by using pyrene as fluorescent probe.[40] In detail, the CACs of micelles were related with the emission intensity ratio of the third and first bands (I3/I1) in the fluorescence spectrum of pyrene. The value of CAC was assessed from the first inflection point in the curve of absorption intensity ratio of I3/I1 versus the logarithm of concentration.[41] The CAC values of TCAD NPs was calculated to be 23.4 μg/mL approximately (Figure S4, ESI).

In vitro DOX and Ce6 release

To demonstrate the acid-sensitivity of TCAD @Ce6 NPs, the *in vitro* DOX and Ce6 release behavior of TCAD@Ce6 NPs was measured by dialysis in PBS at pH 7.4, 6.5, and 5.5 at 37℃, respectively. The results of cumulative release curves revealed that DOX and Ce6 without significant burst release from TCAD @Ce6 NPs in PBS (pH 7.4), suggesting a good stability of TCAD @Ce6 NPs in normal physiological tissues conditions (Figure 2C). Nevertheless, at a mild acidic environment pH 6.5 or even 5.5, which simulated microenvironment of the tumor tissular and intracellular, respectively, the cumulative release of DOX and Ce6 was accelerated dramatically. When incubated with PBS (pH = 5.5), the cumulative release of DOX and Ce6 from the TCAD@Ce6 NPs was higher than that observed when incubated with PBS (pH = 6.5). On this basis, the TCAD@Ce6 NPs will release more of their drug cargo in the endo/lysosomal vesicles (pH 5.5) than in the solid tumor extracellular environment (pH 6.5). Moreover, most of the TCAD@Ce6 NPs may be taken up by the tumor cells before releasing their drug cargo. In this case, even if some of the drug cargo were released in the solid tumor extracellular environment they may enter the tumor cells by passive diffusion, which may have little influence on cellular uptake and therapeutic efficacy. [42, 43] All the results may attribute to the expedite hydrolysis of the acid-sensitive linker under acidic environment. This acid-sensitivity release of TCAD @Ce6 NPs makes them an interesting tool for clinic tumor chemo-photodynamic combination therapy that may minimize the damage of healthy tissues and maximize the therapeutic efficacy. The Ce6 was wrapped into the interior of TCAD @Ce6 NPs, which might cause the aggregation of Ce6 by π-π and hydrophobic interactions, resulting in a dramatic reduction of NIR fluorescence by self-quenching. That is, the recovery of NIR fluorescence of Ce6 from TCAD @Ce6 NPs can be correlated to the release of Ce6. To estimate the intracellular NIR fluorescence recovery of Ce6 in TCAD @Ce6 NPs, NIR fluorescence images of TCAD @Ce6 NPs after co-incubation with or without A549 cells at different time points were analysed (Figure 2D). In the absence of A549 cells, the fluorescence changed little in the medium over time. Noteworthily, the fluorescence intensity increased dramatically with the extending of incubation time in the presence of A549 cells, suggesting that the Ce6 was gradually released from TCAD @Ce6 NPs inside of the cell, resulting in the fluorescence recovery of Ce6. Moreover, the fluorescence of Ce6 in the TCAD@Ce6 NPs was dramatically lower than free Ce6 due to the self-quenching effect before being treated with

mild acidic PBS (pH=5.5). However, after 24h incubation in mild acidic PBS (pH=5.5), an obvious increase of fluorescence intensity of Ce6 was detected (Figure S5, ESI). Therefore, we came to a conclusion, the acid-sensitivity TCAD@Ce6 NPs would self-quenching the phototoxicity in blood circulation to weaken side effects and recover phototoxicity in the target tumor acid microenvironment.

Cellular uptake and intracellular distribution

The cellular uptake behavior of TCAD and TCAD@Ce6 nanoparticles was evaluated by confocal laser scanning microscopy (CLSM) and flow cytometry (FCM) toward A549 cells. The Flow cytometry analysis after 4 h incubation (Figure 3A & Figure 3B) indicated that about 21.5% of A549 cells displayed a fluorescence signal from DOX in TCAD NPs, which is higher than that detected in free DOX (about 15.5%). However, after 12 hours incubation, the same analysis revealed that the ratio of A549 cells with fluorescence signal of DOX when exposed to TCAD NPs was increased to about 92.7%, which was higher than that of free DOX (about 64.1%). Meanwhile, the fluorescence signal intensity of DOX from TCAD NPs was similar with that of TCAD@Ce6 NPs in A549 cells with incubation time prolonged. Predictably, the cells co-cultured with TCAD@Ce6 for 4 h or 12 h, exhibited significantly higher ratios of Ce6 fluorescence signal when compared to those incubated with free Ce6. It demonstrated that TCAD@Ce6 NPs would enhance cellular uptake capability of Ce6 and DOX in A549 cells, compared with free Ce6 and free DOX. Overall, these phenomenon may owe to the efficient endocytosis and rapid intracellular DOX and Ce6 release, which were induced by the intracellular acidic microenvironment-triggered hydrolysis of the amide linker in TCAD and TCAD@Ce6.[44]

DOX, is a well known and widely used anticancer drug, that shows anti-cancer effect by damaging the DNA structure in nuclei.[45] Whereas Ce6, a common photosensitizer, tends to locate in the cytoplasm.[46] Next, TCAD NPs and TCAD@Ce6 NPs were incubated with A549 cells for 4 h and 12 h, respectively, confocal microscope images were utilized to visually show the cellular internalization and the intracellular release of DOX and Ce6. As shown in the Figure 3C, the green fluorescence and red fluorescence were used to localize the DOX and Ce6, respectively. Hoechst 33342 was used to stain the nuclei (blue). For free DOX, after being incubated with A549 cells for 4 h, very slight green fluorescence was detected, suggesting that free DOX entered the cells at low quantities. When incubation times were prolonged to 12 h, the green fluorescence of free DOX was spread all over the cells and the intensity of green fluorescence was enhanced (Figure S6, ESI). In contrast, in the case of TCAD NPs and TCAD@ Ce6 NPs, DOX was observed highly accumulated in nuclei as compared with free DOX, when incubated with A549 cells for 4 h (Figure S6 & Figure 3C). Meanwhile, a significant increase of green fluorescence intensity of DOX in nuclei was detected, after TCAD NPs and TCAD@Ce6 NPs were incubated with A549 cells for 12 h. These observations demonstrated TCAD NPs may be an attractive way to assist DOX circumvent the multidrug resistance, enter into the cytoplasm and then diffuse into the nucleus. Additionally, the red fluorescence intensity of Ce6 in cytoplasm from the TCAD@ Ce6 NPs was higher than that of free Ce6, and increased remarkably with the extension of incubation time. In a word, the confocal microscope images obtained are consistent with the results obtained by flow cytometry. The enhanced cell uptake of TCAD and TCAD@Ce6 NPs may take advantage of endocytosis efficiently rather than passive diffusion through the cell membrane of free DOX and free Ce6.[47]

***In vitro* cellular toxicity**

MTT assay was executed to detect the *in vitro* cellular proliferation inhibitions of free DOX, and TCAD NPs against A549 cells. As shown in Figure 4A, TCAD NPs exhibited more notable antiproliferation efficacy on A549 cells *in vitro* than that of equivalent free DOX, after 24 h or 48 h co-incubation. The trends became more significant with incubation time prolong. The result was also verified by apoptosis assay (Figure 4B). These may take advantage of the cellular uptake enhancement of TCAD NPs and the quick release of DOX at acid intracellular microenvironment as demonstrated above.

Singlet oxygen would induce the damage of cellular constituents and subsequent cell death, which can denote the phototoxicity of nanoparticles.[20] The extracellular singlet oxygen production was detected by a singlet oxygen sensor green (SOSG) reagent. TCAD@Ce6 NPs exhibited the increased singlet oxygen generation capability along with prolongation of irradiation time (Figure S7, ESI). Moreover, DCFH-DA staining method was employed to examine the intracellular singlet oxygen production for actual research the phototoxicity of intracellular nanoparticles. As expected, detected with flow cytometry assay, the TCAD@Ce6 NPs caused the most remarkable singlet oxygen production under irradiation compared with free Ce6 under irradiation and TCAD@Ce6 NPs without irradiation (Figure S8, ESI). Subsequently, the cytotoxic efficacy and the efficiency of of chemo-photodynamic combination therapy of TCAD@Ce6 NPs on A549 cells with or without laser irradiation was further quantified by MTT assay and apoptosis assay. As shown in Figure 4C, relative to treated with free Ce6/laser, a significantly decreased survival ratio of A549 cells was detected when treated with TCAD@Ce6 NPs/laser. In addition, after 24h incubation, the survival ratio of A549 cells was 71.2% and 66.44% when treated with free Ce6 (4.0 μg/mL) upon laser irradiation for 3min (Figure 4C) and TCAD NPs (equivalent DOX 6.0 μg/mL) (Figure 4A), respectively, while the cell survival ratio of A549 cells suddenly decreased to 15.73% when exposed to TCAD@Ce6 NPs (equivalent Ce6 4.0 μg/mL and equivalent DOX 5.86 μg/mL) plus laser irradiation for 3 min (Figure 4C). That is, with the same concentrations of Ce6 plus laser irradiation or DOX, the TCAD@Ce6 NPs would lead to the mortality rate as high as about 2.9 times of that treated with the free Ce6, and about 2.5 times higher than that treated with TCAD NPs. All the results indicated the combination therapy resulted in more striking tumor treatment effect than chemo or photodynamic treatment alone.

The flow cytometry assay reconfirmed that minimal apoptosis and necrosis of A549 cells (mortality ratio <11%) were induced by free Ce6 in the dark or cells with only laser exposure. Meanwhile, the ratio of apoptosis and necrosis was increased to 80% when the cells was exposed to TCAD@Ce6 NPs plus laser irradiation, while slight increase cells apoptosis was detected when treated with free Ce6 plus laser irradiation (Figure 4D).

Furthermore, the cell was stained with Calcein-AM and PI to visually detect the photodamge, when cultured with free Ce6 and TCAD@Ce6 NPs with or without laser. The red fluorescence of PI and the green fluorescence of Calcein-AM were on the behalf of dead and live cells, respectively. As anticipated, after 3 min of irradiation, there was weak red fluorescence emitted from the cell treated with free Ce6, suggesting little cells were photodamged (Figure 4E). The low cellular uptake and the little intracellular singlet oxygen production may be the likely reason. Nevertheless, the TCAD@Ce6 NPs treated cells performed striking red fluorescent signal with laser irradiation. That is, the phototoxicity of TCAD@Ce6 NPs is higher than free Ce6 upon the NIR laser. The experimental results of singlet oxygen detection test, MTT assay, apoptosis assay and Calcein-AM and PI staining assay were consistent, revealing TCAD@Ce6 NPs may be a promising ways for DOX delivery and PDT treatment.

Tumor-targeting evaluation of the TCAD@Ce6

The intrinsic NIR fluorescence of Ce6 allows for detecting the tumor targeting and *in vivo* distribution of TCAD@Ce6 NPs in A549 tumor-bearing nude mice by NIR imaging approach. The Ce6 and TCAD@Ce6 NPs were tail vein injection into the A549 tumor-bearing nude mice to monitor its time dependent distribution *in vivo*. As shown in Figure 5A, free Ce6 as a kind of small dye molecules, absence of tumor targeting, mainly accumulated in the liver and was rapidly catabolized from mice. Whereas, the TCAD @Ce6 NPs exhibited relatively higher tumor targeting efficiency and relatively longer tumor retention time. That is TCAD@Ce6 NPs for PDT would prolong phototoxicity duration and enhance the tumor accumulation of Ce6. More importantly, despite strong NIR fluorescence signal was observed in liver after 2 h injection, the tumor site of TCAD@Ce6 NPs treated mice exerted the higher NIR fluorescence than free Ce6 treated ones. As time goes on, the accumulation of fluorescence signal was gradually reduced in liver while gradually increased in the tumor. The fluorescence intensity signals of tumor reached maximum at 12 h post injection and with faint decrease after 24 h injection, suggesting TCAD@Ce6 NPs were not subject to rapid metabolism from mice and excellent *in vivo* tumor-specific by the EPR effect. Furthermore, the mean fluorescence intensity of tumor treated with TCAD@Ce6 and free Ce6 was quantified (Figure 5B). The fluorescence accumulation in tumor of Ce6 in TCAD@Ce6 NPs was about 18 fold higher than free Ce6, 12 h post-injection. In addition, *in vitro* fluorescence images of organs (heart, liver, spleen, lung, and kidney) excised from mice (sacrificed at 24 h post-injection) were executed to intuitively observe the tumor targeting efficacy and tissue distribution of free Ce6 and TCAD@Ce6 NPs. Predictably, similar to the *in vivo* images, TCAD@Ce6 NPs were much more inclined to accumulate to tumor than stay in normal organs, indicating they may possess high therapeutic efficiency and low side effect for PDT (Figure 5C). Nevertheless, the florescence of free Ce6 was mainly remained in liver. Similar with free DOX, the TCAD@Ce6 NPs were mainly captured and metabolized by liver and kidney, rusulting in the strong fluorescence signals of TCAD@Ce6 NPs in liver and kidney.[4] The mean fluorescence intensity of organ and tumor was also quantified (Figure 5D).

Photodynamic therapeutic efficacy of TCAD@Ce6 NPs in tumor-bearing mice

To evaluate the chemo-photodynamic therapeutic efficacy of TCAD@ Ce6 NPs *in vivo*, phosphate buffer solution (PBS), free DOX, TCAD NPs, free Ce6 and TCAD@ Ce6 NPs were intravenously injected into A549 tumor-bearing mice when the tumor size grew to 90 – 100 mm^3. Whereafter, to monitor the photodynamic therapeutic efficacy, the tumor site of free Ce6 and TCAD@Ce6 NPs treated mice were irradiated with a NIR laser (633 nm, 50 mW/cm^2) for 30 min, after 12 h injection. As showed in figure S9, at 4 days post-irradiation, TCAD@Ce6 NPs plus laser treated mice showed lightly hemorrhagic injury at the irradiation tumor site, while free Ce6/laser or PBS/laser treated group has no noticeable phototoxicity damage. After 14 days, normal tissue had already regenerated at necrotic scar site of tumor. The change of tumor volume and body weight of tumor-bearing mice was monitored every 3 days within 18 days. As showed in figure 6A, NIR laser irradiation may not significantly inhibit the A549 tumor growth, when A549 tumor-bearing mices were treated with saline. Because of short blood circulation time and less tumor accumulation of free Ce6, the growth of tumor tissue of free Ce6 treated mice was not successfully suppressed. Importantly, the tumor was repressed by the singlet oxygen generated by TCAD@Ce6 NPs upon irradiation, that is not present in TCAD NPs. It must be acknowledged that the combined TCAD@Ce6/laser treatment was remarkably more efficient in suppressing tumor growth than treatment with free Ce6/laser or TCAD NPs. Unlike free Ce6 or TCAD NPs alone, this observation may be caused by the long retention time and tumor targeting efficacy of TCAD@Ce6 NPs, where the tumor was inhibited by the combination of chemo and photodynamic therapy effects. Moreover, the tumor inhibition efficacy of TCAD NPs and free DOX was significantly different, which may attribution to the efficient tumor accumulation of acid-sensitivity TCAD by EPR effect and quick excretion by glomerular filtration of free DOX.[5] Interestingly, TCAD@Ce6 NPs with laser irradiation, which efficient combination Ce6-mediated phototoxicity and DOX-mediated chemotherapy, led to effective inhibition of tumor growth with the average tumor volume was 95.29% smaller than that of the saline control mice on the 18 days post-irradiation. All the results confirming the superiority of chemo-photodynamic combined therapy of TCAD@Ce6 NPs. As we all know, the body weight of the mouse can indicate the treatments-induced toxicity. As shown in Figure 6 B, the body weight loss of mice treated with TCAD NPs was relatively slight compared with those treated with free DOX which had an obvious weight loss. This revealed that TCAD NPs is a relative safety prodrug for tumor therapy. Meanwhile, no significant variation of body weight was observed after treatment, indicating that the chemo-photodynamic therapeutic of TCAD@Ce6 NPs may hardly induce the treatment toxicity. Moreover, Haematoxylin and eosin (H&E) staining of organs was executed to histopathological examinations. As expected, the TCAD@Ce6 NPs groups showed neither obvious pathological abnormality or lesion in heart, spleen, and kidney, nor obvious liver damage (Figure S10). Overall, the combination treatment of TCAD@Ce6 NPs upon laser irradiation was demonstrated remarkable anticancer efficacy with little side effect.

Conclusions

In summary, we successfully prepared a novel well-defined acid-sensitivity nanoparticles TCAD@Ce6 NPs by self-assembly process, for tumor NIR imaging and chemo-photodynamic combination therapy. The TCAD@Ce6 NPs exhibited stability in water and could be easily hydrolyzed in acidic microenvironment of tumor. Compared with free Ce6 and DOX, it could significantly enhance cellular uptake of DOX and Ce6 and induce higher phototoxicity upon NIR laser irradiation. Based on EPR effect, TCAD@Ce6 NPs could accumulate in tumor sites effectively for tumor NIR fluorescent imaging and efficient inhibition of the growth of A549 tumor under laser irradiation *in vivo*. Hight performance TCAD@Ce6 NPs can sever as prodrugs for DOX delivery and specific combined chemo-photodynamic therapy, and exhibit great potential in applications such as tumor NIR fluorescent imaging and simultaneous combined chemo-photodynamic therapy in near future.

Acknowledgements

This work is supported by National Key Basic Research Program (973 Project) (Project No.2010CB933901), National Natural Scientific Foundation of China (Grant Nos. 81225010, 81028009, and 31170961), 863 project of China (Project No. 2012AA022703 and 2014AA020700), and Shanghai Science and Technology Fund (13NM1401500).

Notes and references

[a] *Department of Bio-Nano Science and Engineering, Key Laboratory for Thin Film and Microfabrication of Ministry of Education, Institute of Micro/Nano Science and Technology, Shanghai Jiao Tong University, Shanghai 200240, P.R. China. E-mail: dxcui@sjtu.edu.cn (D.Cui)*

[b] *School of Biomedical Engineering, Shanghai Jiao Tong University, Shanghai 200240, P.R. China*

cInstituto de Nanociencia de Aragón,Universidad de Zaragoza,Spain

† Electronic Supplementary Information (ESI) available: Additional experimental results. See DOI: 10.1039/b000000x/

1. M. Chidambaram, R. Manavalan and K. Kathiresan, *J. Pharm. Pharm. Sci.*, 2011, **14**, 67-77.
2. R. H. Blum and S. K. Carter, *Ann. Intern. Med.*, 1974, **80**, 249-259.
3. C. Du, D. Deng, L. Shan, S. Wan, J. Cao, J. Tian, S. Achilefu and Y. Gu, *Biomaterials*, 2013, **34**, 3087-3097.
4. D. Sun, J. Ding, C. Xiao, J. Chen, X. Zhuang and X. Chen, *ACS Appl. Mater. Interfaces*, 2014, **6**, 21202-21214.
5. J. Ding, W. Xu, Y. Zhang, D. Sun, C. Xiao, D. Liu, X. Zhu and X. Chen, *J. Controlled Release*, 2013, **172**, 444-455.
6. O. A. AL-SHABANAH, H. A. EL-KASHEF, O. A. BADARY, A. M. AL-BEKAIRI and M. M. ELMAZAR, *Pharmacol. Res.*, 2000, **41**, 31-37.
7. N. Duhem, F. Danhier, V. Pourcelle, J.-M. Schumers, O. Bertrand, C. c. S. LeDuff, S. Hoeppener, U. S. Schubert, J.-F. o. Gohy and J. Marchand-Brynaert, *Bioconjugate Chem.*, 2013, **25**, 72-81.
8. L. Pan, Q. He, J. Liu, Y. Chen, M. Ma, L. Zhang and J. Shi, *J. Am. Chem. Soc.*, 2012, **134**, 5722-5725.
9. M. Zheng, C. Yue, Y. Ma, P. Gong, P. Zhao, C. Zheng, Z. Sheng, P. Zhang, Z. Wang and L. Cai, *Acs Nano*, 2013, **7**, 2056-2067.
10. L. Zhang, S. Zhu, L. Qian, Y. Pei, Y. Qiu and Y. Jiang, *Eur. J. Pharm. Biopharm.*, 2011, **79**, 232-240.
11. C.-M. J. Hu and L. Zhang, *Biochem. Pharmacol.*, 2012, **83**, 1104-1111.
12. A. R. Afshar, R. D. Patel and R. D. Jager, *Invest. Ophthalmol. Visual Sci.*, 2012, **53**, 400-400.
13. A. Jhaveri, P. Deshpande and V. Torchilin, *J. Controlled Release*, 2014, **190**, 352-370.
14. Z. Wang, R. Ma, L. Yan, X. Chen and G. Zhu, *Chem. Commun.*, 2015, **51**, 11587-11590.
15. S. Wang, A. Riedinger, H. Li, C. Fu, H. Liu, L. Li, T. Liu, L. Tan, M. J. Barthel and G. Pugliese, *ACS nano*, 2015, **9**, 1788-1800.
16. W. W. L. Chin, P. W. S. Heng, P. S. P. Thong, R. Bhuvaneswari, W. Hirt, S. Kuenzel, K. C. Soo and M. Olivo, *Eur. J. Pharm. Biopharm.*, 2008, **69**, 1083-1093.
17. R. Bonnett, *Chem. Soc. Rev.*, 1995, **24**, 19-33.
18. Z. Zhao, S. Shi, Y. Huang, S. Tang and X. Chen, *ACS Appl. Mater. Interfaces*, 2014, **6**, 8878-8885.
19. P. Liu, C. Yue, Z. Sheng, G. Gao, M. Li, H. Yi, C. Zheng, B. Wang and L. Cai, *Polym. Chem.*, 2014, **5**, 874-881.
20. C. Zhang, C. Li, Y. Liu, J. Zhang, C. Bao, S. Liang, Q. Wang, Y. Yang, H. Fu and K. Wang, *Adv. Funct. Mater.*, 2015, **25**, 1314-1325.
21. H. Isakau, M. Parkhats, V. Knyukshto, B. Dzhagarov, E. Petrov and P. Petrov, *J. Photochem. Photobiol., B*, 2008, **92**, 165-174.
22. Y. Li, Y. Yu, L. Kang and Y. Lu, *Int. J. Clin. Exp. Med.*, 2014, **7**, 4867.
23. H. Y. Yoon, H. Koo, K. Y. Choi, S. J. Lee, K. Kim, I. C. Kwon, J. F. Leary, K. Park, S. H. Yuk and J. H. Park, *Biomaterials*, 2012, **33**, 3980-3989.
24. A. Yuan, B. Laing, Y. Hu and X. Ming, *Chem. Commun.*, 2015, **51**, 6678-6680.
25. V. Karabanovas, A. Skripka, J. Valanciunaite, R. Kubiliute, V. Poderys and R. Rotomskis, *J. Nanopart. Res.*, 2014, **16**, 1-8.
26. J.-H. Park, Y.-H. Moon, I.-S. Bang, Y.-C. Kim, S.-A. Kim, S.-G. Ahn and J.-H. Yoon, *Lasers Med Sci.*, 2010, **25**, 705-710.
27. J. R. Fischer, K. R. Harkin and L. Freeman, *Vet Ther: Res Appl Vet Med.*, 2001, **3**, 465-473.
28. N. Cao and S.-S. Feng, *Biomaterials*, 2008, **29**, 3856-3865.
29. M. Sadoqi, C. Lau-Cam and S. Wu, *J. Colloid Interface Sci.*, 2009, **333**, 585-589.
30. H.-J. Youk, E. Lee, M.-K. Choi, Y.-J. Lee, J. H. Chung, S.-H. Kim, C.-H. Lee and S.-J. Lim, *J. Controlled Release*, 2005, **107**, 43-52.
31. G. Tian, X. Zheng, X. Zhang, W. Yin, J. Yu, D. Wang, Z. Zhang, X. Yang, Z. Gu and Y. Zhao, *Biomaterials*, 2015, **40**, 107-116.
32. Y. Mi, J. Zhao and S.-S. Feng, *J. Controlled Release*, 2013, **169**, 185-192.
33. L. Milane, S. Ganesh, S. Shah, Z.-f. Duan and M. Amiji, *J. Controlled Release*, 2011, **155**, 237-247.
34. F.-Q. Hu, L.-N. Liu, Y.-Z. Du and H. Yuan, *Biomaterials*, 2009, **30**, 6955-6963.
35. G. Tian, W. Ren, L. Yan, S. Jian, Z. Gu, L. Zhou, S. Jin, W. Yin, S. Li and Y. Zhao, *Small*, 2013, **9**, 1929-1938.
36. M. S. Muthu, D. T. Leong, L. Mei and S.-S. Feng, *Theranostics*, 2014, **4**, 660.
37. R. Rotomskis, J. Valanciunaite, A. Skripka, S. Steponkiene, G. Spogis, S. Bagdonas and G. Streckyte, *Lith. J. Phys.*, 2013, **53**.
38. S. Mitra, U. Gaur, P. Ghosh and A. Maitra, *J. Controlled Release*, 2001, **74**, 317-323.
39. Z. Gao, A. N. Lukyanov, A. Singhal and V. P. Torchilin, *Nano Lett.*, 2002, **2**, 979-982.
40. G. Kwon, M. Naito, M. Yokoyama, T. Okano, Y. Sakurai and K. Kataoka, *Langmuir*, 1993, **9**, 945-949.
41. P. Huang, D. Wang, Y. Su, W. Huang, Y. Zhou, D. Cui, X. Zhu and D. Yan, *J. Am. Chem. Soc.*, 2014, **136**, 11748-11756.
42. H. S. Han, J. Lee, H. R. Kim, S. Y. Chae, M. Kim, G. Saravanakumar, H. Y. Yoon, D. G. You, H. Ko and K. Kim, *J. Controlled Release*, 2013, **168**, 105-114.
43. H. Wang, F. Xu, Y. Wang, X. Liu, Q. Jin and J. Ji, *Polym. Chem.*, 2013, **4**, 3012-3019.
44. M. Li, Z. Tang, S. Lv, W. Song, H. Hong, X. Jing, Y. Zhang and X. Chen, *Biomaterials*, 2014, **35**, 3851-3864.
45. M. Yoshida, I. Shiojima, H. Ikeda and I. Komuro, *J. Mol. Cell. Cardiol.*, 2009, **47**, 698-705.
46. H. Jeong, M. Huh, S. J. Lee, H. Koo, I. C. Kwon, S. Y. Jeong and K. Kim, *Theranostics*, 2011, **1**, 230.
47. Y.-Z. Zhao, C.-Z. Sun, C.-T. Lu, D.-D. Dai, H.-F. Lv, Y. Wu, C.-W. Wan, L.-J. Chen, M. Lin and X.-K. Li, *Cancer Lett.*, 2011, **311**, 187-194.

Figure captions

Table 1. Characteristics of TCAD@Ce6 NPs after Ce6 loading.

D/P ratio[a]	EE%	DL (%)	Diameter(nm)[b]
1:10	98.50%	8.96%	157.20±3.1
1:20	85.25%	14.89%	160.00±1.6

[a] D/P ratio = weight of Ce6/weight of TCAD.
[b] Measured using dynamic light scattering (DLS), data represent mean ±SD, n = 3.

Scheme 1. Schematic illustration of the preparation of the TCAD@Ce6 NPs and their applications *in vitro* and *in vivo*. CA: Cis-Aconitic anhydride.

Figure 1. ^{1}H NMR and FT-IR spectra of DOX (DMSO-d_6), CAD (DMSO-d_6),TPGS ($CDCl_3$), and TCAD ($CDCl_3$).

Figure 2. Characterization of the nanoprobes. (A). Morphology of TCAD@Ce6 NPs observed by TEM and size distribution measured by DLS; (B).Colloid stability test of TCAD and TCAD @Ce6 NPs in water; (C). Cumulative release DOX and Ce6 from TCAD@Ce6 NPs in different pH; (D). The NIR image of TCAD@Ce6 NPs in culture medium (10% FBS) without cells (M) or co-incubated with A549 cells (M+C) for different times.

Figure 3. Cellular uptake efficacy and localization. Flow cytometry separate analysis (A) and integral analysis (B) of cellular uptake of free Ce6, free DOX, TCAD and TCAD@Ce6 NPs for 4 h and 12h, respectively; (C).Confocal images of A549 cells exposed to free Ce6 or TCAD@Ce6 NPs for 4 h and 12 h, respectively. Scale bar, 100 μm.

Figure 4. *In vitro* cellular toxicity. MTT assay quantitative evaluation (A) and flow cytometry analysis (B) of cell survival for A549 cells treated with free DOX and TCAD NPs for 24 h and 48 h, respectively; Dark toxicity and photocytoxicity of free Ce6 and TCAD@Ce6 NPs towards A549 cells for 24 h, analyzed by MTT assay (C) and flow cytometry (D), respectively; (E).Detection of photodamage by fluorescence microscopy using fluorescent probes (double-staining with calcein PI and calcein-M). Dead cells: red fluorescence of PI, live cells: green fluorescence of calcein-AM. The data are shown as mean ±SD (n = 3).

Figure 5. *In vivo* fluorescence imaging and biodistribution of Ce6 and TCAD@Ce6 NPs. (A). *In vivo* time-dependent whole body fluorescence imaging of A549 tumor-bearing mice after

intravenous injection of free Ce6 and TCAD@Ce6 NPs; B. Quantification of average fluorescence signals in the tumor site of (A). (C). *In vitro* fluorescence images of major organs and tumors of mice after intravenous injection of free Ce6 or TCAD@Ce6 NPs over a period of 24 h; (D) Quantification of average fluorescence signals of (C). The data are shown as mean ±SD (n = 3)

Figure 6. *In vivo* chemo-photodynamic therapy TCAD@Ce6 NPs. Tumor volume growth curves (A) and body weight evolutions curves (B) of the mice after treatment with free DOX, TCAD NPs, free Ce6/laser irradiation or TCAD@Ce6 NPs/ laser irradiation. Data were showed as a mean ± SD (n = 3).

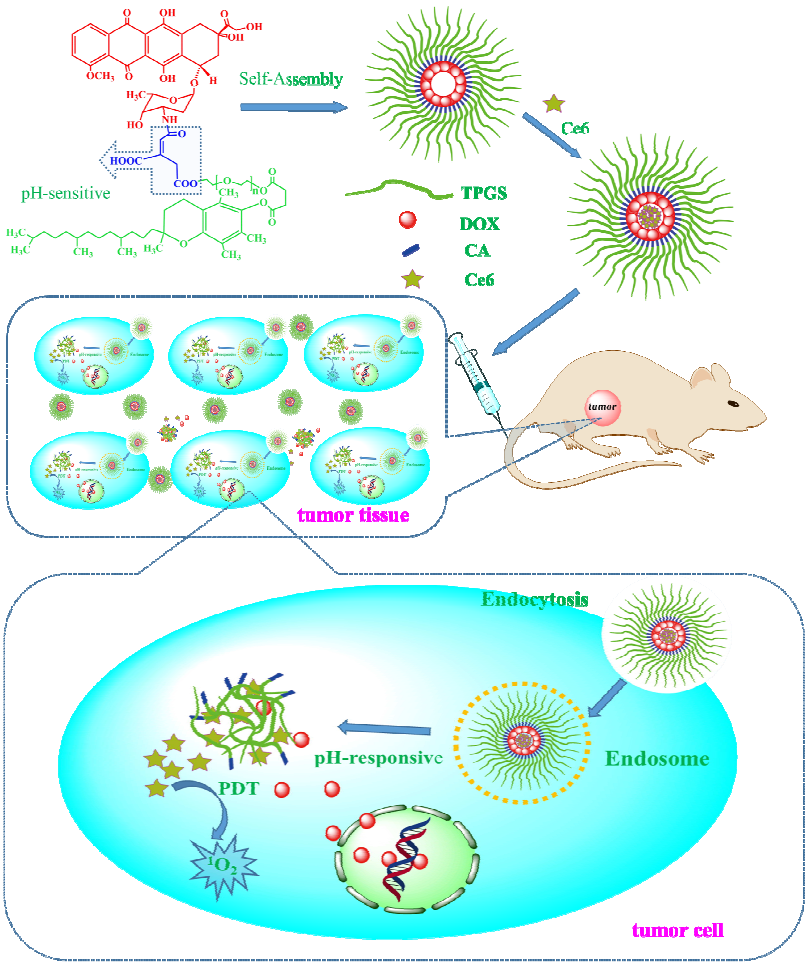

Scheme 1
Hou. et al.

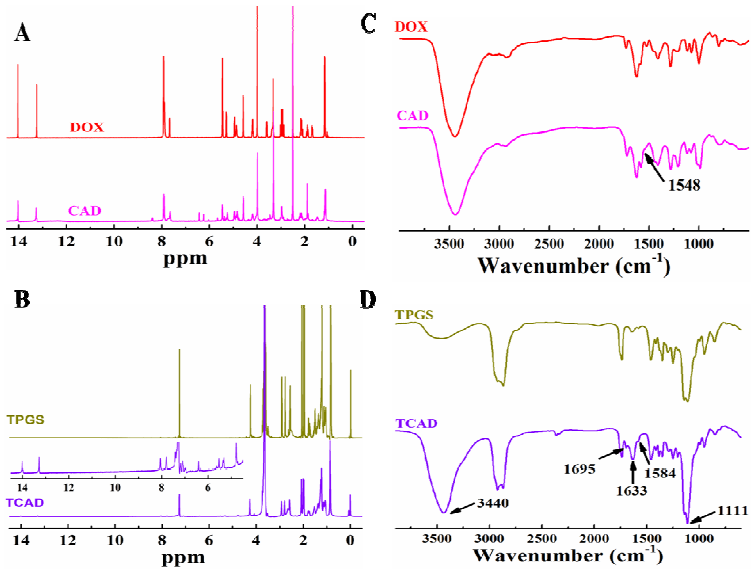

Figure 1
Hou. et al.

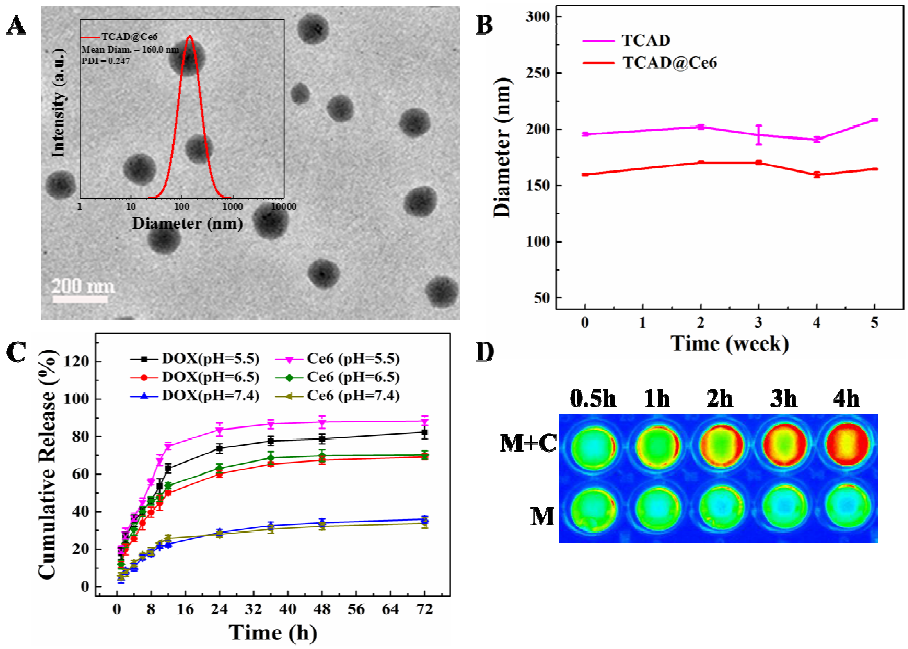

Figure 2
Hou. et al.

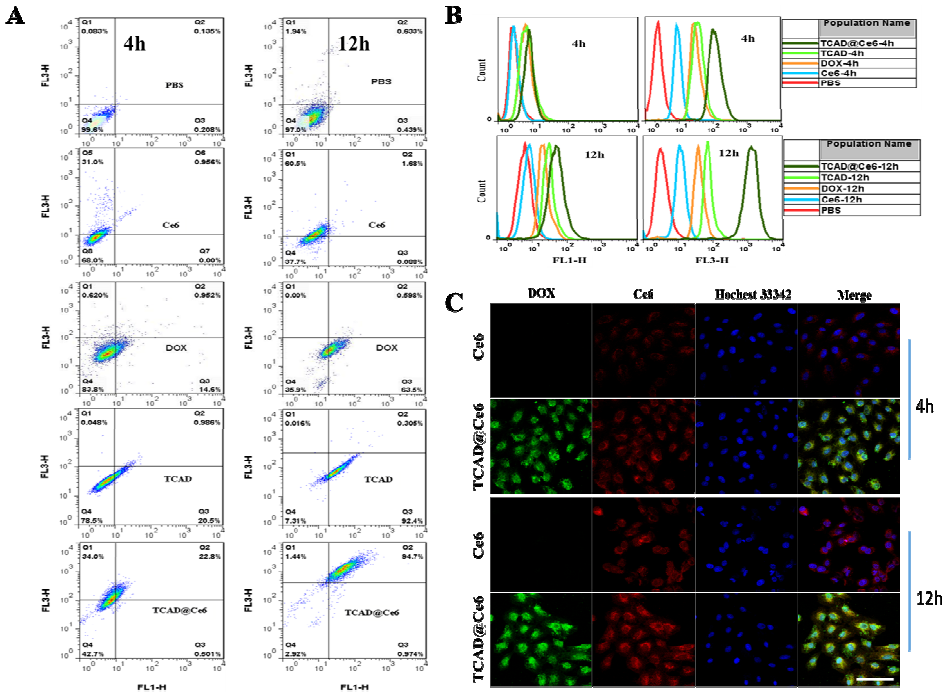

Figure 3
Hou. et al

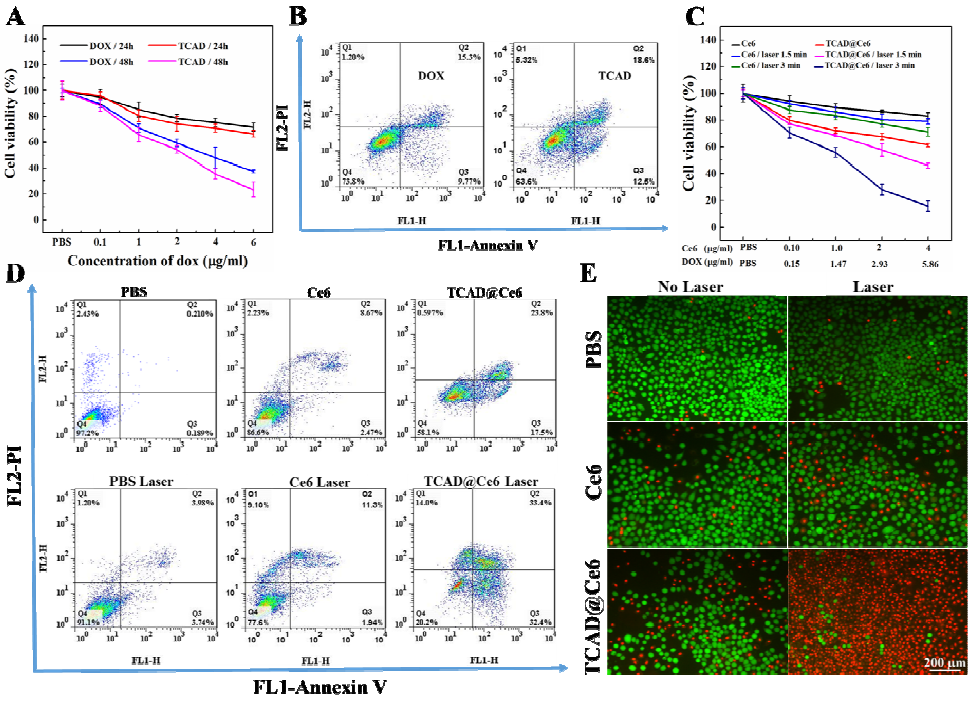

Figure 4
Hou. et al.

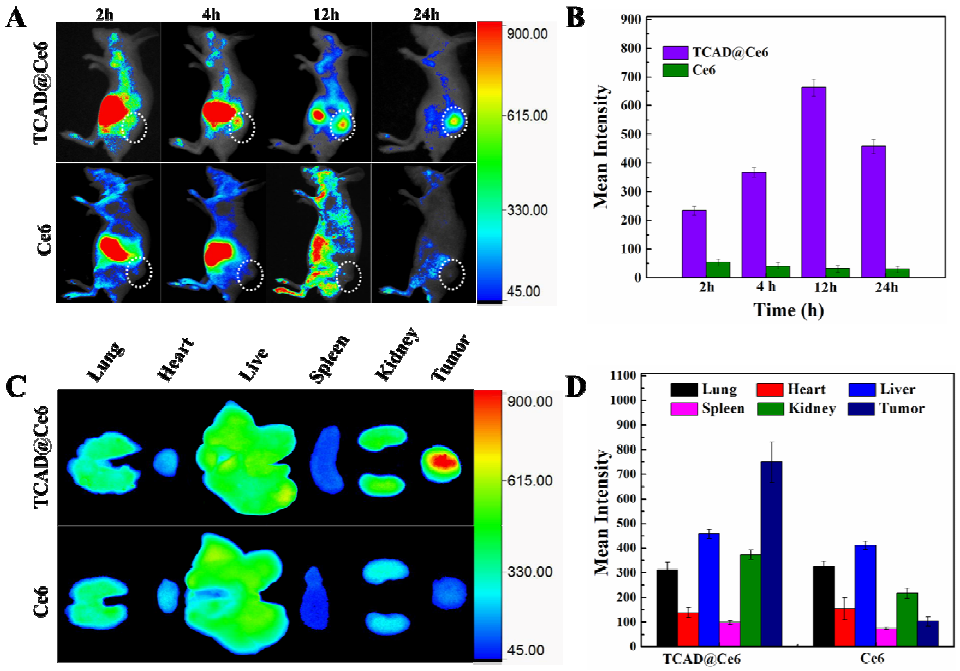

Figure 5
Hou. et al.

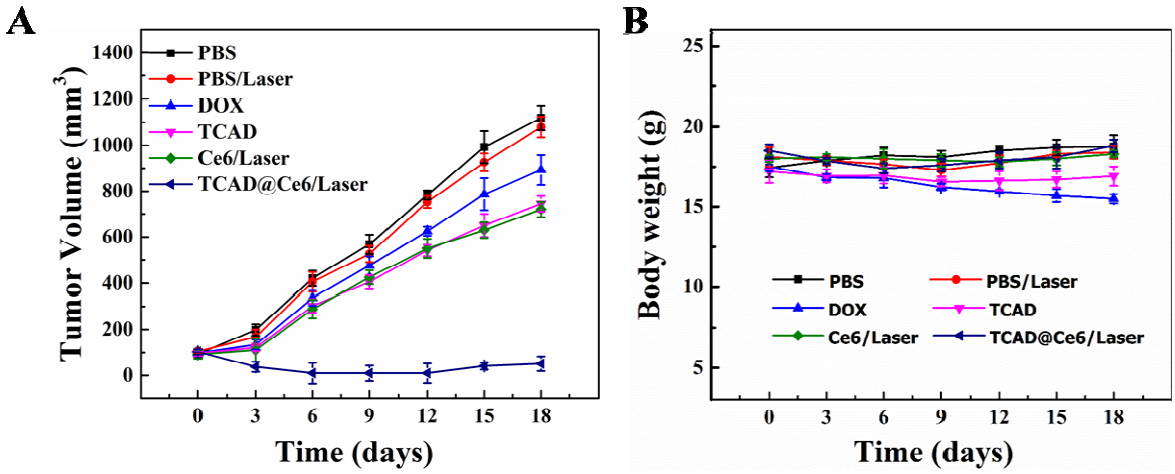

Figure 6
Hou. et al.